Discover Applied Sciences

Research

Laser photostability of chitosan coated gold-GO nanocomposite and its role as a nano-therapeutic agent for control breast cancer growth

Marwa A. Ramadan[1] · Sara Gad[2] · Marwa Sharaky[3,4] · Amna H. Faid[5]

Received: 26 October 2023 / Accepted: 11 March 2024
Published online: 26 March 2024

Abstract

Background As the global cancer burden increases, it is critical to develop alternative treatments that produce minimal side effects, owing to its optical, thermal, and biological anticancer and biomedical applications of graphene and its nanocomposites. researchers have devoted the past few years to developing graphene/polymer and graphene/metal nanocomposites.

Materials and methods Here a simple, highly stable, non-toxic, eco- friendly chitosan gold nanoparticles (Cs-AuNPs) and its nanocomposites with graphene oxide nanosheets (GO) to form novel photostable (GO/AuNPs) nanocomposites. The prepared nanomaterials were characterized by UV–Vis, FTIRs, TEM and Raman as shown in graphical abstract. In addition, the anticancer efficiency of the prepared nanomaterials in breast cell lines (MCF7, T47D, MDA-MB-468 and MDA-MB-231) using SRP assay were evaluated.

Results Results revealed that Cs-AuNPs bound with the GO sheets via electrostatic interaction with high stability with uniform decoration. A new FTIRs peak of high intensity was found in the GO/Au nanocomposite confirming the decoration of Cs-AuNPs on the surface of the GO layers. GO/Au nanocomposite has a significant cytotoxic effect on breast cell lines as compared to GO only.

Conclusion This work opens perceptions for translational applications of GO/Au nanocomposite on cancer cell lines, future work is to use the prepared nanocomposite in photothermal chemotherapy combined treatment.

✉ Marwa A. Ramadan, marwali_mus@cu.edu.eg; Sara Gad, sgad@srtacity.sci.eg; Marwa Sharaky, marwa.sharaky@nci.cu.edu.eg; Amna H. Faid, amna.hussein@cu.edu.eg | [1]Department of Laser Application in Metrology, Photochemistry and Agriculture, National Institute for Laser Enhanced Science (NILES) Cairo University (CU), Cairo, Egypt. [2]Electronic Materials Research Department, Advanced Technology and New Materials Research Institute, City of Scientific Research and Technological Applications (SRTA-City), Alexandria, Egypt. [3]Pharmacology Unit, Cancer Biology Department, National Cancer Institute (NCI), Cairo University, Cairo, Egypt. [4]Biochemistry Department-Faculty ofPharmacy, Ahram Canadian University, Giza, Egypt. [5]Department of Laser Science and Interaction, National Institute for Laser Enhanced Science (NILES) Cairo University (CU), Cairo, Egypt.

Graphical abstract

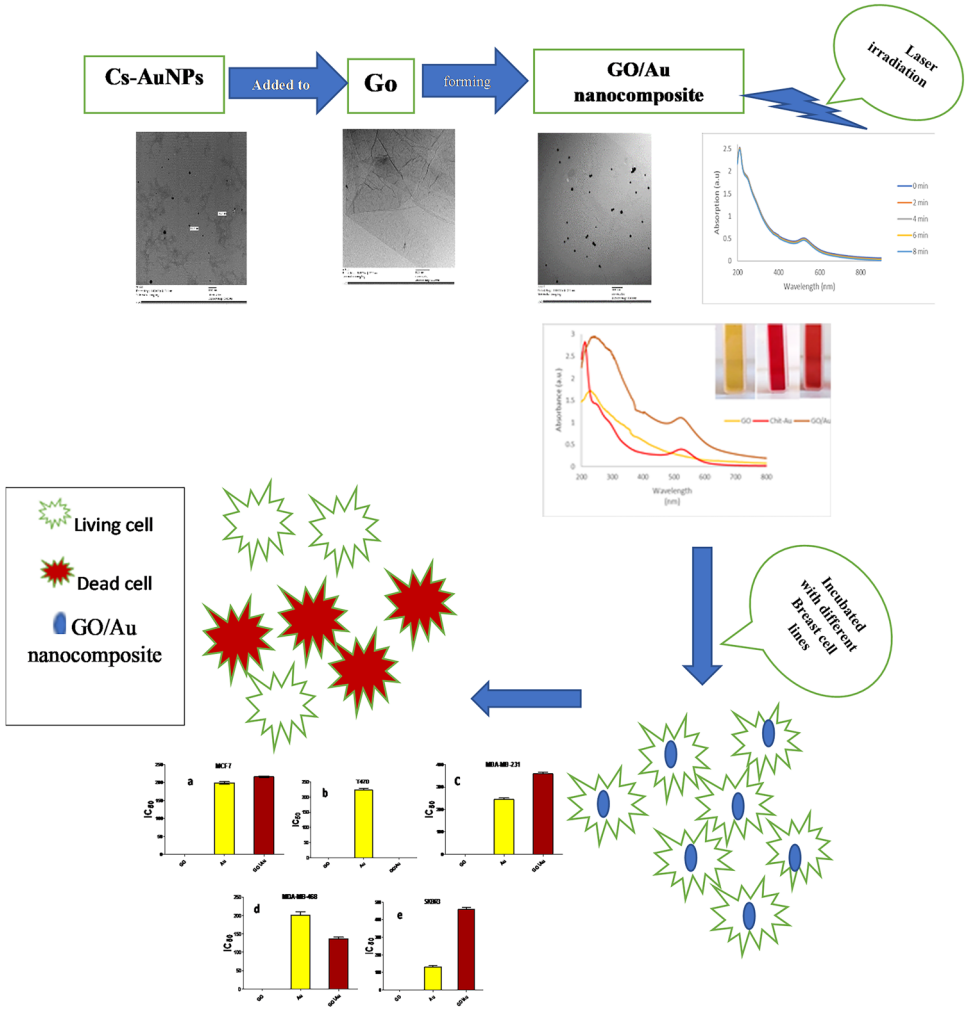

Article highlights

- Chitosan reduced gold nanoparticles were successfully prepared and incorporated on graphene oxide nanosheets.
- Chitosan reduced gold nanoparticles reduce the viability of the cell population after 48h exposure with the lower 50 percentage viability concentration.
- Incorporation of Chitosan reduced gold nanoparticles on graphene oxide enhance the cytotoxic effect of graphene oxide consequently graphene oxide / gold nanoparticles nanocomposite has a significant cytotoxicity effective against all tested breast cancer cells.

Keywords Chitosan coated AuNPs · GO/Au nanocomposite · Laser photostability · Raman spectroscopy · Breast cancer cell lines

1 Introduction

Graphene oxide/metal nanocomposites perform better than metallic nanoparticles and graphene oxide nanosheets (GO) alone because of their complementary effects [1–6]. Therefore, efforts have been concentrated on decorating GO surfaces with AuNPs and investigating their potential uses in a variety of industries, including

sensors, cancer detection, photothermal treatment, and drug administration. Graphene-constructed nanocomposites are increasingly existence taken into account for their potential biological uses [7–9]. The benefit of NPs' tiny size is that they may continuously enter cells through the plasma membrane, and their unique surface characteristics enable them to interact only with certain biomolecules in the cytoplasm, bodily fluids, or tissues [10–17]. An interesting characteristic of AuNPs called surface plasmon resonance (SPR) has been associated with a number of surface-enhanced Raman scattering (SERS)-based biomedical applications [18–22] including bio-imaging and biomolecule identification. Theragnostic for cancer, particularly for cancer diagnostic and bio sensing applications, can benefit from the conjugation of GO with a noble metal like Au because of its specific features [23]. We explore the usage of GO/ Au nanocomposites in cancer treatment on breast cancer cell models in this article because of their great features. One of the critical elements for diagnosis and therapy is the biocompatibility and clearance of AuNPs. Pharmacological and toxicological investigations have demonstrated the biocompatibility of graphene-based derivatives, with hydrophilic GO being favored over pure graphene [6, 24]. The characteristics of the GO/AuNPs nanocomposite may also be significantly enhanced by functionalizing graphene, making them potent stages for the creation of cheap, sensitive, and quick drug delivery structures, biosensors, and photothermal treatment. Combined hard work from researchers are being made to enhance the synthetic processes for investigating the unique features of these innovative constituents in biomedical applications in diagnostics and treatments [25–30]. Interesting biological actions are also displayed by chitosan (Cs) and chitosan nanoparticles, including antibacterial activity, disease resistance in plants, and various stimulating or inhibitory activities towards various human cell types [11, 31]. These factors make chitosan an extensively utilized substance in a variety of industries, such as medical, pharmaceuticals, nutrition, and agriculture [22, 32]. Due to its role as a dispersion and ability to prevent metal particle agglomeration, chitosan was used to create valuable metal nanocomposites [33–35]. It is thus of tremendous interest to create chitosan-coated gold (Cs-Au) and combine it with GO. In most investigations up until this point, dangerous reducing agents like sodium borohydride and hydrazine were employed in the production of GO/Au nanocomposite. These synthesis processes are intricate and include several phases [36]. The performance of the GO/MNPs nanocomposites is decreased by the application of surfactants because they are powerfully absorbed on the exterior of the metallic NPs. The production of GO/MNPs nanocomposites via physical and chemical processes has been the focus of efforts [37]. Green synthesis techniques have not been widely used in investigations to create GO/Au nanocomposites [38] and their biological activity in human cancer cell models. It is critical to identify potential novel therapeutic compounds that have the potential to greatly increase cancer cell apoptosis. People's interest in nanomedicine is still stimulated by these features.

In present work GO, Cs-AuNPs, and GO/Au nanocomposite were quickly, cheaply, and eco-friendly prepared. In addition, the efficiency of the prepared nanomaterials in dealing breast cancer cell line was done.

2 Material and methods

2.1 Synthesis of graphene oxide nanosheets (GO)

Nanosheets of GO were synthesized from oxidation of graphite using a modified Hummers method as in our prior research [7, 37, 39].

2.2 Green synthesis of chitosan-coated gold nanoparticles (CS-AuNPs) [14, 40]

Cs-AuNPs have been manufactured by means of chitosan as a reducing/capping mediator by thermal reduction methods [41]. CS-AuNPs was prepared by reducing tetrachloroaurate with chitosan, in this method 5ml of 10^{-3}M solution of $HAuCl_4.3H_2O$ (99.9%, Sigma-Aldrich) was reduced by 40ml chitosan 0.2% acetic acid at 100˚C fabricating red solution. The Prepared Cs-AuNPs were dried using lypholizer.

2.3 Synthesis of GO/Au nanocomposite

GO/Au nanocomposites are synthesized via the ex-situ method by slowly adding 10 mL Cs-AuNPs with 10 mL GO solution in a beaker glass under continuous stirring. The volume ratio between GO and Cs-AuNPs is 1:1, then the mixture homogenized with stirring for 30 min and sonication for 30 min at ambient temperature, then GO/Au nanocomposite dried using lypholizer.

2.4 Laser photostability of Au@CsNs

Diode Pumped Solid State (DPSS) laser 532 nm with 150 mW was used to irradiate GO/Au nanocomposite for 2, 4, 6 and 8 min then the absorption spectra were observed before and after exposure.

2.5 Characterization of GO, (Cs-AuNPs) and GO/Au nanocomposite

The absorption spectrum for nanomaterials were measured by means of UV–Vis-NIR spectrophotometer (Cary 5000, Agilent, Santa Clara, USA), The analysis was performed via quartz cell with wavelength range of 250–1000 nm. Morphology was analyzed by a high-resolution Transmission electron Microscope (HRTEM, Tecnai, G20, FEI, Almelo, Netherlands). Droplets from diluted nanomaterials were let fall on carbon-coated copper grid and dried. FTIRs were done using FTIR spectrometer (4100 Jasco-Japan) (400–4400 cm^{-1}). Raman spectroscopy for the nanomaterials were systematically analyzed by (Raman Senterra II, Germany) with a laser wavelength of 532 nm.

2.6 Cytotoxicity assay

Here, a plate of the obtainable cell lines was confirmed for their sensitivity to the prepared nanomaterials. Different concentrations GO, (Cs-AuNPs) and GO/Au nanocomposite were used for all tested cell lines. Human breast tumor cell line (T47D, MCF7, SKBR3, MDA-MB-231 and MDA-MB-468) were used in this study. It was gained from the American Type Culture Collection (ATCC, Minnesota USA). The tumor cell line maintained at National Cancer Institute (NCI), Cairo, Egypt. The antitumor activities of the prepared nanomaterials and cell lines were estimated by sulphorhodamine-B (SRB) assay [42]. Cells were seeded at a density of 3×10^3 cells/well in 96-well microtiter plates then attached for 24 h before incubation with nanomaterials. Subsequent, treated with of changing concentrations of GO, (Cs-AuNPs) and GO/Au nanocomposite (200, 400 and 600 ug/ml) µg/ml for T47D, MCF7, SKBR3, MDA-MB-231 and MDA-MB-468 cells. For individual concentration, three wells were used, and incubation was continued for 48 h. DMSO acted as control vehicle (1% v/v). Latterly, cells were fixed with 20% trichloroacetic acid then stained with 0.4% SRB dye. The optical density (O.D.) of individually well was analyzed spectrophotometrically at 570 nm by means of ELISA microplate reader (TECAN sunrise™, Germany). The mean survival fraction at each drug concentration was calculated as follows: O.D. of the treated cells/O.D. of the control cells. The IC50 (concentration that produce 50% of cell growth inhibition) value of each drug was calculated (Graph Pad Prizm software, version 5) soft wear [42].

2.7 Statistical analysis

Statistics are obtainable as mean ± standard deviation. Statistical analysis was performed using Graph Pad software Prism v5. Statistical analysis of transfection assay data performed using Tukey's multiple comparison test. Modifications were statistically significant if $p \leq 0.05$.

3 Results

3.1 Characterization of GO, (Cs-AuNPs) and GO/Au nanocomposite

GO was produced by oxidizing graphite via a modified Hummers method, which is a mixture of potassium permanganate and sulfuric acid, yielding manganese heptoxide (Mn2O7), an active oxidant that oxidizes the unsaturated double bond and form GO. Spectrophotometric measurements of GO solutions Fig. 1, showed absorption in the near-infrared and visible range, but a strong specific absorption peak in the ultraviolet range around 237 nm highly exfoliated ultrathin structure of GO nanosheets with a very smooth surface. AuNPs displayed a surface plasmon-specific resonance at around 530 nm as shown in Fig. 1, which is specific to surface plasmon resonance. Cs-AuNPs interacted with GO layers through electrostatic bonding, physisorption, and charge-transfer interactions. The combination of GO/Au nanocomposites was characterized by UV–visible spectroscopy after incorporation with GO, the peak of Cs-AuNPs displayed a small red-shift from 530 nm to about 540 nm was observed, which provided strong evidence for the persistence of mono-dispersion as well as surface modification. A typical GO band was observed around 240 nm, which indicated that Cs-AuNPs were

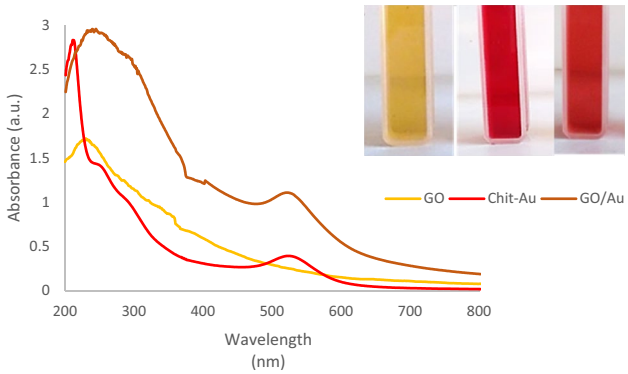

Fig. 1 UV-Absorption and a digital photograph of the GO, Cs-AuNPs and GO/Au nanocomposite

successfully incorporated with GO nanosheets. The GO/Au nanocomposites solutions appear to be uniform and much lighter in color compared with the Cs-AuNPs solution which strongly suggested the incorporation of Cs-AuNPs with GO. So, Cs-AuNPs are tightly attached onto the surface of thin layer of GO through electrostatic interaction to modify the surface property and photothermal performance of Cs-AuNPs.

Figure 2a, TEM image showed highly exfoliated ultrathin structure of GO nanosheets with a very smooth surface and the formation of chitosan stabilized gold nanoparticles was confirmed in Fig. 2b which reveals that spherical Cs-AuNPs with diameters of about 20 ± 5 nm. In Fig. 2c, showed the incorporation of Cs-AuNPs with GO and Cs-AuNPs tightly attached onto the surface of thin layer of GO through electrostatic interaction.

In Fig. 3a, upon laser irradiation has no change in the absorption peaks which confirm the stability of GO/Au nanocomposites. Figure 3b, the broadband FTIR spectrum for Cs-AuNPs, GO and GO/Au nanocomposites, the FTIR-GO spectrum shows broad and intense absorption peaks in 1723 and 1245 cm^{-1}, the characteristic –OH, –C=O absorption peaks in the GO/Au nanocomposite decrease indicating a successful conversion of GO into a GO/Au nanocomposite. Thus, as observed, a new peak of high intensity was found in the GO/Au nanocomposite, confirming the decoration of Cs-AuNPs on the surface of the GO layers. In Fig. 3c, the Raman spectroscopy of Cs-AuNPs have three bands that can be observed at, 1350, 1580, and 2700 cm^{-1}, which are D, G, and 2D peaks of graphene shell.

3.2 Effect of Cs-AuNPs and GO/Au nanocomposite on viability of breast cancer cell lines

With the aim of estimating the GO/Au nanocomposite potential for biomedical application, cytotoxicity of GO, Cs-AuNPs and GO/AuNPs were evaluated against breast cell lines (MDA-MB-231, T47D, SKBR3, MCF7, MDA-MB-468 cells) at changed concentrations after 48 h using the SRP assay. GO, AuNPs and GO/Au nanocomposite influenced a concentration-dependent cell viability decrease.

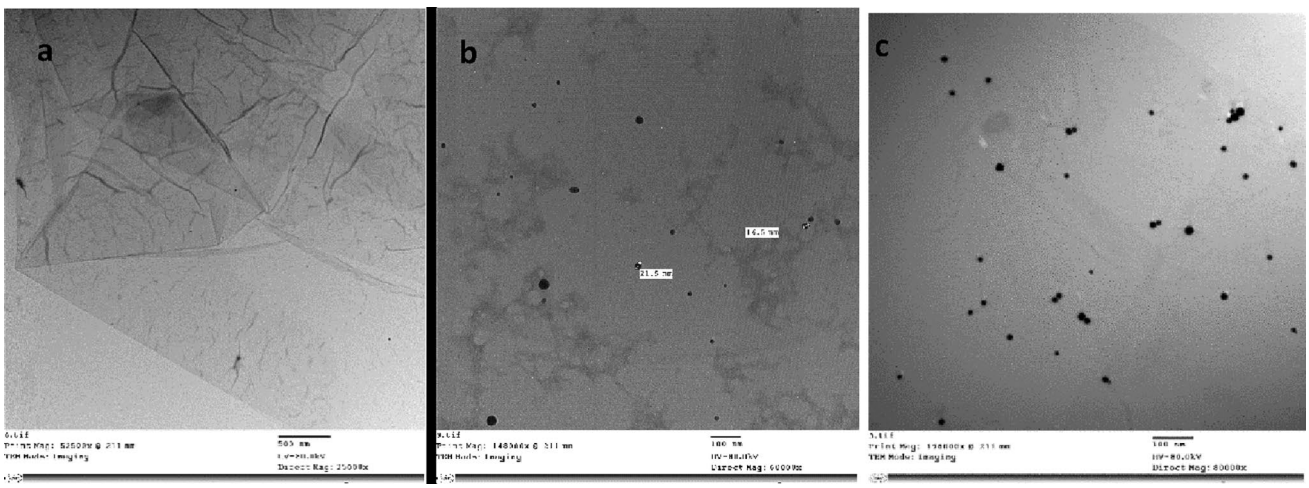

Fig. 2 TEM images of the **a** GO **b** Cs-AuNPs **c** GO/Au nanocomposite (magnification 100,500 nm)

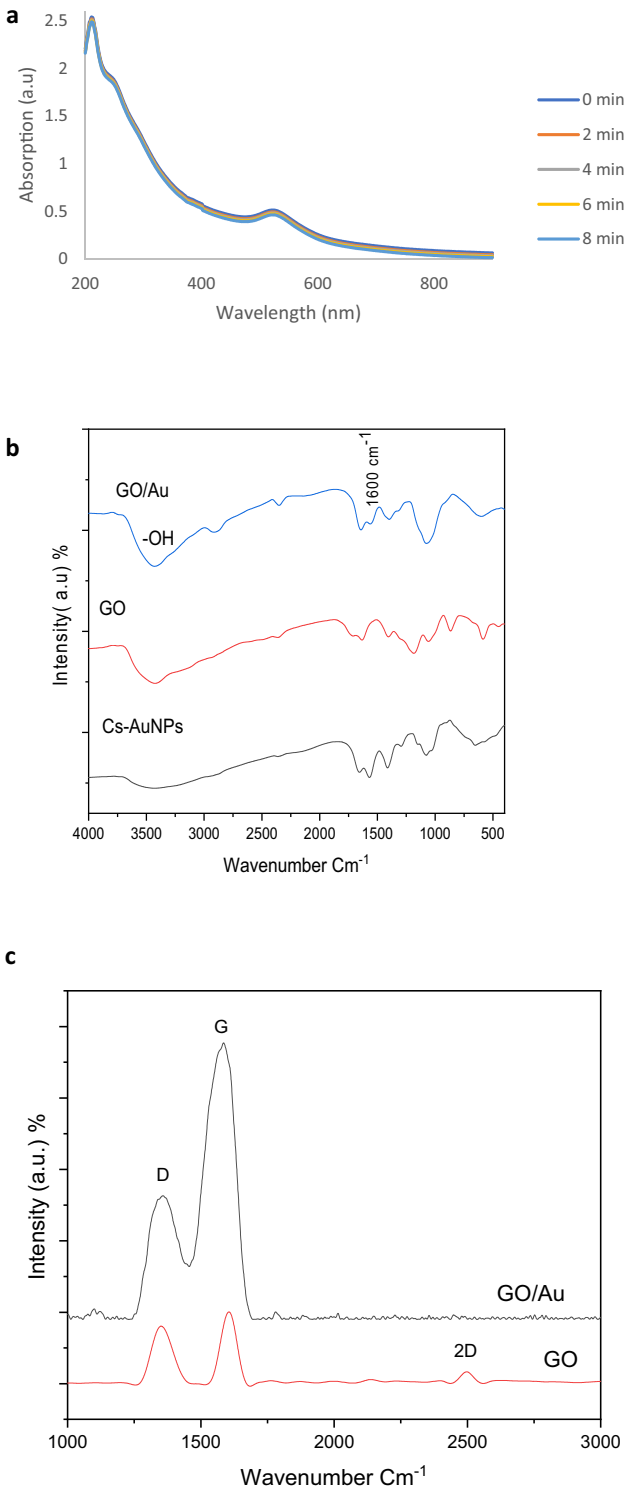

Fig. 3 **a** laser photostability of GO/Au nanocomposites **b** FTIR spectra of samples **c** Raman spectra of samples

Outcomes of the current study exposed that all the tested breast cancer cell lines were affected by (200,400, and 600 ug/ml) concentrations of GO, Cs-AuNPs, GO/Au nanocomposites that were used in this study Table 1, Figs. 4 and 5, showed that samples has IC50 on all tested cell line which is (T47D, MCF7, SKBR3, MDA-MB-231 and MDA-MB-468 cells) after 48 h. Cs-AuNPs showed the strongest effect in all breast cell lines.

Table 1 The IC50 breast cancer cell lines after 48h incubation with Cs-AuNPs and GO/Au nanocomposite

Cell lines	MCF7		T47D		MDA-MB-231		MDA-MB-468		SKBR3	
	IC50 (µg/ml)	SD	IC50 (µg/ml)	SD	IC50 (µg/ml)	SD	IC50 (µg/ml)	SD	IC50 (µg/ml)	SD
Cs-AuNPs	199	3.70	224	5.00	245	6.00	201	9.00	131	7.00
GO\Au nanocomposite	216	2.40	–	0.00	359	7.00	136	5.00	458	12.00

4 Discussion

Mostly, gold nanoparticles are produced via numerous agents, such as sodium borohydride, chitosan, and even alcohol. The second-most prevalent polysaccharide in nature, chitosan, has reducing and capping properties [41], Because of its advantageous biological characteristics, including small harmfulness and sensitivity to biodegradation, chitosan was chosen in this investigation. It has a negative charge and serves as an electrostatic stabilizer for polyelectrolytes. Chitosan's amino group functions as a stabilizer and a reducing agent. Chitosan alone may convert $AuCl^{4-}$ ions to zero-valent gold nanoparticles without the use of another reducing agent. Since the amine groups are primarily involved in the reduction of tetrachloroauric acid and the capping of AuNPs in chitosan, these AuNPs displayed a surface plasmon-specific resonance at around 530 nm Fig. 1a. Protonation of chitosan amino groups occurs in an acidic medium ($R\text{-}NH3^{+}$) on superficial and forms a framework for absorbing oppositely charged $AuCl^{4-}$ ions. The electrostatic attraction among the positively charged chitosan amino groups and the $AuCl^{4-}$ negatively charged ions promotes nanoparticle formation and confers high stability to the nanoparticles. After reduction by chitosan chains, the Au cores bound to AuNPs on chitosan due to van der Waals forces and attraction among amino groups and Au particles. The chitosan-coated AuNPs exhibited a surface plasmon-specific resonance at ~ 530 nm, as amine groups are mainly involved in tetrachloroauric acid reduction Fig. 1a. Protonation of chitosan amino groups happens in an acidic medium ($R\text{-}NH^{3+}$) and forms a framework for absorbing oppositely charged $AuCl^{4-}$ ions. The attraction among the positively charged amino groups of chitosan and the negatively charged $AuCl^{4-}$ ions promotes nanoparticle formation and confers high stability to the nanoparticles. After reduction by chitosan chains, Au cores bound to AuNPs and self-assembled on the surface of chitosan through van der Waals forces and high attraction between amino groups and Au particles.

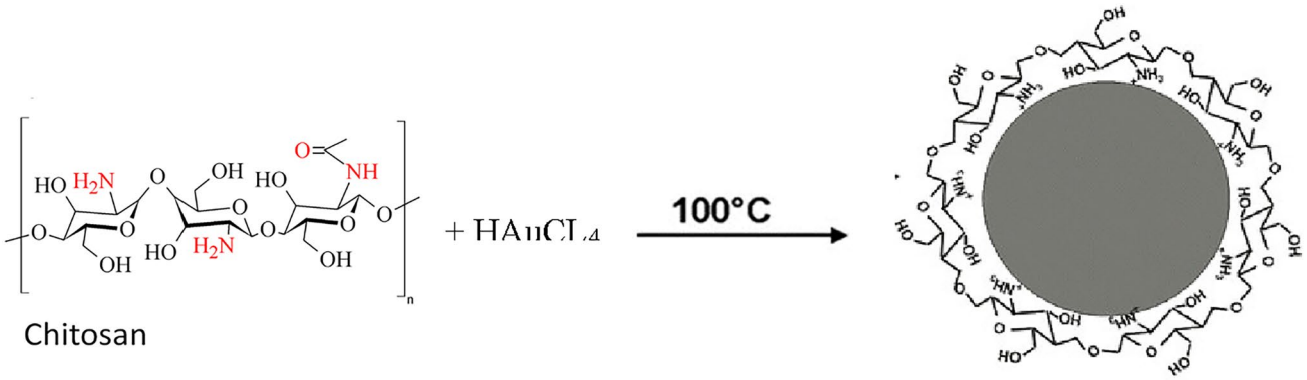

Equation 1: Proposed mechanism of reaction between CS and HAuCL4forming AuNPs.

Numerous approaches for the synthesis of various GO/Au nanocomposites have been reported, including chemical reduction, thermal reduction, photochemical reduction, and sonochemical reduction. In most of these approaches, water- or ethanol-based GO suspensions are reacted with metal precursors in the presence of reducing agents, sodium citrate or ascorbic acid, to achieve simultaneous reduction of metal ions to form nanocomposites. produce materials. $HAuCl_4$ is a commonly used metal precursor for the synthesis of Cs-AuNPs. In an ex-situ method, Cs-AuNPs and GO nanoparticles are synthesized separately and attached to graphene sheets using electrostatic bonds, p–p bonds, hydrogen bonds, or van der Waals interactions for binding. This method ensures a uniform size distribution and it is possible to control the amount of Cs-AuNPs on the graph [43]. Therefore, the ex situ process represents a promising technique to overcome

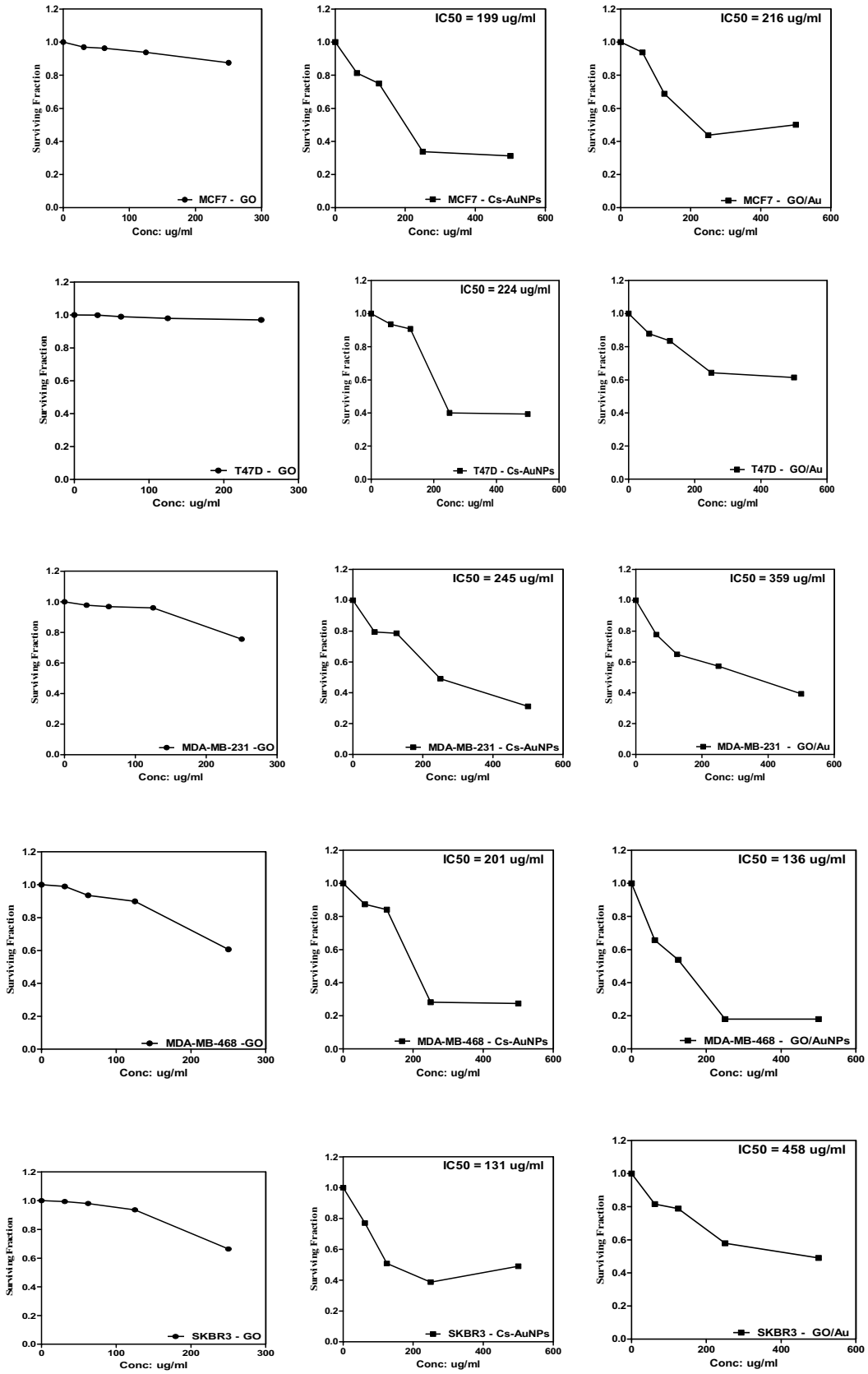

Fig. 4 Cytotoxicity at changed concentrations (µg/ml) of GO, Cs-AuNPs and GO/Au nanocomposite on breast cell lines (MCF7, T47D, MDA-MB-231, MDA-MB-468 and SKBR3) after incubation for 48 h

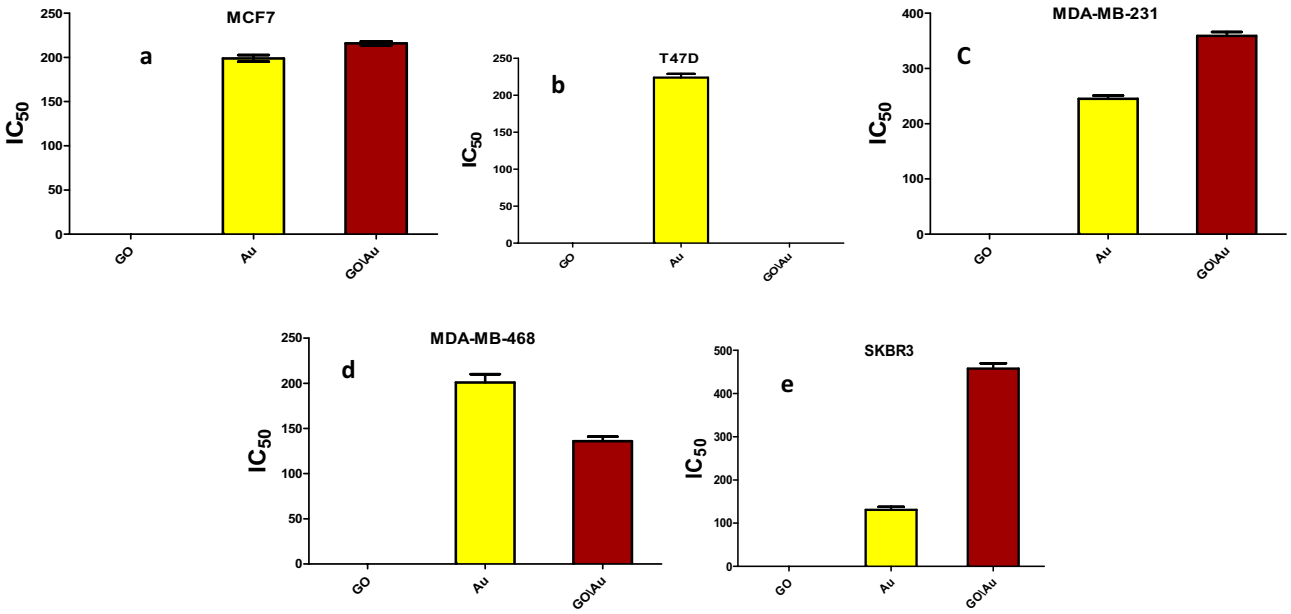

Fig. 5 IC50)µg/ml (values for GO, Cs-AuNPs and GO/Au nanocomposite after incubation for 48h with breast cell lines **a** MCF7 cell line **b** T47D cell line **c** MDA-MB-231 cell line **d** MDA-MB-468 cell line **e** SKBR3 cell line

the difficulties encountered in the in situ synthesis of nanocomposites [43]. Furthermore, the GO sheets acted as an exceptional support and stabilizer for the synthesis of Cs-AuNPs without significant aggregation [44, 45]. can provide a range of p-p interactions between Cs-AuNPs and GO. Figure 3b the broadband FTIR spectrum at 3330 cm^{-1} is from OH stretching vibrations and confirms the existence of hydroxyl groups on GO. In addition, FTIR-GO spectrum shows broad and intense absorption peaks in 1723 and 1245 cm^{-1} equivalent to the stretching frequencies of the –C=O (carbonyl) and C–O (epoxide) groups, respectively. The band at 1730 cm^{-1} is mainly caused by the stretching vibrations of the carboxyl groups. The contribution of other carbonyl functional groups probably overlaps this band by conversely, the characteristic –OH, –C=O absorption peaks in the GO/Au nanocomposite decrease indicating a successful conversion of GO into a GO/Au nanocomposite. It shows strong absorption bands at 1063 cm^{-1}, 1113 cm^{-1}, and 1658 cm^{-1}, which are ascribed to vibrations of the C–O–C epoxy stretch of the phenolic hydroxyl group, the C–OH stretch, and the GO carbonyl groups, respectively. The observed peak at 1420 cm^{-1} characteristics to the bending mode of the –OHGO group [46, 47]. Furthermore, the peak at 1600 cm^{-1} in GO confirms the occurrence of sp2 hybridization. Upon incorporation of GO into Cs-AuNPs, the GO band disappeared, which means that almost all GO particles were quantitatively covered by Cs-AuNPs. Thus, as observed, a new peak of high intensity was found in the GO/Au nanocomposite, confirming the decoration of Cs-AuNPs on the surface of the GO layers. In Fig. 3c, the Raman spectroscopy of Cs-AuNPs have three bands that can be observed at, 1350, 1580, and 2700 cm^{-1}, which are D, G, and 2D peaks of graphene shell. The D and 2D bands are the structures of graphitic sp2 materials, and the G band is interrelated to the defects of graphene, shows that the shell is not perfect graphene [48]. The D band 1350 cm^{-1} is related to the phono mode A1g and the G band 1580 cm^{-1} is correlated to the phonon mode E2g that show the degree of graphitization and the 2D band is very sensitive to changes in the number of GO layers [49, 50]. It can be seen that there is a re-establishment of a conjugated graphene network after the GO has been successfully decorated with Cs-AuNPs [51].

Previous research has shown that GO has anticancer properties in the biomedical field. According to the previous explanation, the cytotoxic effects of GO on MDA-MB-468, SKBR3, MDA-MB-231, MCF7, and T47D at 250 g/mL were 40%, 38%, 22%, 15%, and less than 5%, respectively. This effect was caused by GO's potent physical interactions with the phospholipid layer, which led to the loss of plasma membrane integrity and its resulting injury. According to reports, GO assemble inside of cells after entering and physically disrupting the plasma membrane [39]. As shown in Table 1, Cs-AuNPs may be enter cells via receptor-mediated endocytosis and phagocytosis pathways. Cs-AuNPs produced a decrease in cell viability that reached IC50. Table 1 The IC50 breast cancer cell lines after 48h incubation with Cs-AuNPs and GO/Au nanocomposite [52]. It has been established that chitosan and AuNPs both cause cell cycle arrest in the G1 and S phases of cancer cells, respectively. Even though AuNPs and chitosan individually cause cell cycle arrest in several cancer cell lines, this suggests that cell viability reduction is caused by cell death induction. Previous investigations using different

kinds of AuNPs have also shown that ROS production is necessary for inducing cell death. Furthermore, a prior work stated that Cs-AuNPs induced ROS production in cancer cells [53, 54]. The viability of the cell population was reduced 50% after 48h exposure with the lower IC50 concentration (131 µg/mL), indicating the biocompatibility for the Cs-AuNPs. However, GO/Au nanocomposite has the optimum concentration up to 50 µg/mL because of the non-toxicity of GO/Au nanocomposite to breast cell lines up to this concentration. With increasing GO/Au nanocomposite concentration from 50 to 500 µg/mL cytotoxicity has increased reaching IC50 value on breast cell lines are shown in Table 1. Our results were in agreement with earlier work [4], where they found that GO/Au nanocomposite induced cell cycle arrest which ultimately led to cell death by the essential apoptosis pathway in MCF7 and MDA-MB-231.

5 Conclusion

Here, we successfully prepare Cs-AuNPs using chitosan for production of new GO/Au nanocomposites. UV–Vis, FTIR, Raman, and TEM analysis of the synthesized GO/Au nanocomposite showed that Cs-AuNPs with diameters of around 20 ± 5 nm was placed evenly on GO. GO/Au nanocomposite presented brilliant solubility and photostability. The GO/Au nanocomposite has a significant cytotoxicity and showed highly effective apoptotic activity against breast cancer cells than GO. Our results concluded that the novel synthesized GO/Au nanocomposite can be chosen for photothermal therapy (PTT) studies in the future work using different laser sources especially in NIR. The novel formulation may support the development of improved breast anticancer nanotherapeutics.

Acknowledgements None

Author contributions MAR and AHF designed and performed the experiments, analyzed the data. Sara gad assisted with FTIRs and Raman measurements and MS perform cytotoxicity experiment. MAR and AHF wrote the manuscript in consultation with SG and MS. All authors read and approved the final manuscript.

Funding Open access funding provided by The Science, Technology & Innovation Funding Authority (STDF) in cooperation with The Egyptian Knowledge Bank (EKB).

Availability of data and materials The datasets used and/or analyzed during the current study are available from the corresponding author on reasonable request.

Declarations

Ethics approval and consent to participate Not applicable.

Consent for publication Not Applicable.

Competing interests All the authors declare that they have no competing interests.

References

1. Zedan AF, Moussa S, Terner J, et al. Ultrasmall gold nanoparticles anchored to graphene and enhanced photothermal effects by laser irradiation of gold nanostructures in graphene oxide solutions. ACS Nano. 2013;7:627–36.
2. Ahmad MA, Aslam S, Mustafa F, et al. Synergistic antibacterial activity of surfactant free Ag-GO nanocomposites. Sci Rep. 2021;11(1):196–196.
3. Arun T, Verma SK, Panda PK, et al. Facile synthesized novel hybrid graphene oxide/cobalt ferrite magnetic nanoparticles based surface coating material inhibit bacterial secretion pathway for antibacterial effect. Mater Sci Eng C. 2019;104:109932.
4. Banerjee P, Bandyopadhyay A, Mondal P, et al. Cytotoxic effect of graphene oxide-functionalized gold nanoparticles in human breast cancer cell lines. Nucleus. 2019;62:243–50.

5. Beiranvand M, Farhadi S, Mohammadi A. Graphene Oxide/Hydroxyapatite/Silver (rGO/HAP/Ag) nanocomposite: synthesis, characterization, catalytic and antibacterial activity. Int J Nano Dimens. 2019;10(2):180–94.
6. Ramadan MA, Sharaky M, Gad S, et al. Anticancer effect and laser photostability of ternary graphene oxide/chitosan/silver nanocomposites on various cancer cell lines. Nanomedicine (Lond), 2024.
7. Mostafa MM, Mohamad EA, Ramadan MA, et al. Reduced Graphene Oxide @ Magnetite Nanocomposite and ELFEF effect on Staphylococcus aureus growth inhibition. Egypt J Chem, 2022.
8. Cobos M, De-La-Pinta I, Quindós G, et al. Graphene oxide-silver nanoparticle nanohybrids: synthesis, characterization, and antimicrobial properties. Nanomaterials. 2020;10(2):376.
9. Doghish AS, El-Sayyad GS, Sallam A-AM, et al. Graphene oxide and its nanocomposites with EDTA or chitosan induce apoptosis in MCF-7 human breast cancer. RSC Adv. 2021;11(46):29052–64.
10. Jiang W, Kim BYS, Rutka JT, et al. Nanoparticle-mediated cellular response is size-dependent. Nat Nanotechnol. 2008;3(3):145–50.
11. Ramadan MA, Sharaky M, Faid AH. Ionic gelation synthesis, characterization and cytotoxic evaluation of chitosan nanoparticles on different types of human cancer cell models. Egypt J Chem. 2022;65(2):153–9.
12. Ali MM, Ramadan MA, Ghazawy NA, et al. Photochemical effect of silver nanoparticles on flesh fly larval biological system. Acta Histochem. 2022;124(1):10.
13. Mohamad EA, Ramadan MA, Mostafa MM, et al. Enhancing the antibacterial effect of iron oxide and silver nanoparticles by extremely low frequency electric fields (ELF-EF) against S. aureus. Electromagn Biol Med. 2023;40:1–15.
14. Ahmed AH, Badr YA, Shouman SA, Sliem MA, et al. Green synthesis of Spherical Gold Nanoparticles by Chitosan for 6 Mercaptopurine Delivery. Arab J Nuclear Sci Appl. 2018;51(4):175–80.
15. Ramadan MA, El-Tayeb TA. Photostability, cytotoxicity and photothermal impact of AgNPs, CoAgNC and IOAgNC on HEp-2 laryngeal carcinoma cells. SN Appl Sci. 2023;5(10):253.
16. Mohamad EA, Rageh M, Ezz-Aldoula RA, et al. Examination of the interaction between bovine albumin and gold nanoparticles. Egypt J Chem. 2023;66(13):1689–94.
17. Jabir MS, Nayef UM, Abdul KWK. Polyethylene glycol-functionalized magnetic (Fe_3O_4) nanoparticles: a novel DNA-mediated antibacterial agent. Nano Biomed Eng. 2019;11(1):18–27.
18. Amin RM, Mohamed MB, Ramadan MA, et al. Rapid and sensitive microplate assay for screening the effect of silver and gold nanoparticles on bacteria. Nanomedicine. 2009;4(6):637–43.
19. Faid AH, Shouman SA, Badr YA, et al. Enhanced photothermal heating and combination therapy of gold nanoparticles on a breast cell model. BMC Chem. 2022;16(1):66.
20. Faid AH, Shouman SA, Badr YA, et al. Gold nanoparticles loaded chitosan encapsulate 6-mercaptopurine as a novel nanocomposite for chemo-photothermal therapy on breast cancer. BMC Chem. 2022;16(1):94–94.
21. Faid AH, Shouman SA, Thabet NA, et al. Laser enhanced combinatorial chemo-photothermal therapy of green synthesis gold nanoparticles loaded with 6mercaptopurine on breast cancer model. J Pharm Innov, 2022.
22. Alexeree SMI, Abou-Seri HM, El-Din HES, et al. Green synthesis of silver and iron oxide nanoparticles mediated photothermal effects on Blastocystis hominis. Lasers Med Sci. 2024;39(1):43.
23. Lin D, Wu J, Wang M, et al. Triple signal amplification of graphene film, polybead carried gold nanoparticles as tracing tag and silver deposition for ultrasensitive electrochemical immunosensing. Anal Chem. 2012;84(8):3662–8.
24. Dong HS, Qi SJ. Realising the potential of graphene-based materials for biosurfaces–A future perspective. Biosurf Biotribol. 2015;1(4):229–48.
25. Jabir MS, Nayef UM, Abdulkadhim WK, et al. Supermagnetic Fe3O4-PEG nanoparticles combined with NIR laser and alternating magnetic field as potent anti-cancer agent against human ovarian cancer cells. Mater Res Express. 2019;6(11):115412.
26. Kadhim W, Nayef U, Jabir M. Polyethylene glycol-functionalized magnetic (Fe_3O_4) nanoparticles: a good method for a successful antibacterial therapeutic agent via damage DNA molecule. Surf Rev Lett. 2019;26:1950079.
27. Ibrahim AA, Kareem MM, Al-Noor TH, et al. Pt(II)-Thiocarbohydrazone Complex as Cytotoxic Agent and Apoptosis Inducer in Caov-3 and HT-29 Cells through the P53 and Caspase-8 Pathways. Pharmaceuticals (Basel). 2021;14(6):509.
28. Al-Ziaydi AG, Al-Shammari AM, Hamzah MI, et al. Hexokinase inhibition using D-Mannoheptulose enhances oncolytic newcastle disease virus-mediated killing of breast cancer cells. Cancer Cell Int. 2020;20(1):420.
29. Jabir MS, Rashid TM, Nayef UM, et al. Inhibition of Staphylococcus aureus α-Hemolysin Production Using Nanocurcumin Capped Au@ZnO Nanocomposite. Bioinorg Chem Appl. 2022;2022:2663812.
30. Ali IH, Jabir MS, Al-Shmgani HSA, et al. Pathological And Immunological Study On Infection With Escherichia Coli In ale BALB/c mice. J Phys Conf Ser. 2018.
31. Wei D, Sun W, Qian W, et al. The synthesis of chitosan-based silver nanoparticles and their antibacterial activity. Carbohyd Res. 2009;344(17):2375–82.
32. Jin X, Wang J, Bai J. Synthesis and antimicrobial activity of the Schiff base from chitosan and citral. Carbohyd Res. 2009;344(6):825–9.
33. Shukla SK, Tiwari A. Synthesis of chemical responsive chitosan–grafted-polyaniline bio-composite. Adv Mater Res. 2011;306–307:82–6.
34. Vasconcelos HL, Camargo TP, Gonçalves NS, et al. Chitosan crosslinked with a metal complexing agent: synthesis, characterization and copper(II) ions adsorption. React Funct Polym. 2008;68(2):572–9.
35. Faid AH, Hussein FEZ, Mostafa EM, et al. Hybrid chitosan gold nanoparticles for photothermal therapy and enhanced cytotoxic action of 6-mercaptopurine on breast cancer cell line. Beni-Suef Univ J Basic Appl Sci. 2023;12(1):83.
36. Das MR, Sarma RK, Borah SC, et al. The synthesis of citrate-modified silver nanoparticles in an aqueous suspension of graphene oxide nanosheets and their antibacterial activity. Colloids Surf B. 2013;105:128–36.
37. Salah A, Hassab-Elnaby S, Ramadan MA. Boosting the nonlinear optical absorption of graphene oxide, and gold nanorods by tailoring graphene oxide-gold nanorods hybrids. SN Appl Sci. 2023;5(11):288.
38. Darabdhara G, Das MR, Singh SP, et al. Ag and Au nanoparticles/reduced graphene oxide composite materials: synthesis and application in diagnostics and therapeutics. Adv Coll Interface Sci. 2019;271:101991.

39. Loutfy SA, Salaheldin TA, Ramadan MA, et al. Synthesis, characterization and cytotoxic evaluation of graphene oxide nanosheets. in vitro liver cancer model. Asian Pacific J Cancer Prev. 2017;18:955–61.
40. Sampath M, D Balakumaran M, Kalaichelvan P, et al. Green synthesis of gold nanoparticles for controlled delivery. Adv Mater Lett. 2013;4:933–40.
41. Malathi S, Balakumaran MD, Kalaichelvan PT, et al. Green synthesis of gold nanoparticles for controlled delivery. Adv Mater Lett. 2013;4(12):933–40.
42. Skehan P, Storeng R, Scudiero D, et al. New colorimetric cytotoxicity assay for anticancer-drug screening. JNCI J Nat Cancer Inst. 1990;82(13):1107–12.
43. Bai S, Shen X. Graphene–inorganic nanocomposites. RSC Adv. 2012;2(1):64–98.
44. Liu L, Liu J, Wang Y, et al. Facile synthesis of monodispersed silver nanoparticles on graphene oxide sheets with enhanced antibacterial activity. New J Chem. 2011;35(7):1418–23.
45. Lu G, Mao S, Park S, et al. Facile, noncovalent decoration of graphene oxide sheets with nanocrystals. Nano Res. 2009;2(3):192–200.
46. Vellaichamy B, Periakaruppan P. A facile in situ synthesis of highly active and reusable ternary Ag-PPy-GO nanocomposite for catalytic oxidation of hydroquinone in aqueous solution. J Catal. 2016;344:795–805.
47. Vellaichamy B, Periakaruppan P, Ponnaiah SK. A new in-situ synthesized ternary CuNPs-PANI-GO nano composite for selective detection of carcinogenic hydrazine. Sens Actuators B Chem. 2017;245:156–65.
48. Zhang Y-J, Chen Q-Q, Chen X, et al. Graphene-coated Au nanoparticle-enhanced Raman spectroscopy. J Raman Spectrosc. 2021;52(2):439–45.
49. Zhou J, Gu Y, Deng Z, et al. The dispersion of Au nanorods decorated on graphene oxide nanosheets for solar steam generation. Sustain Mater Technol. 2018;19:e00090.
50. Emadi F, Amini A, Gholami A, et al. Functionalized graphene oxide with chitosan for protein nanocarriers to protect against enzymatic cleavage and retain collagenase activity. Sci Rep. 2017;7:42258–42258.
51. Sahoo PK, Sahoo S, Satpati AK, et al. Solvothermal synthesis of reduced graphene oxide/Au nanocomposite-modified electrode for the determination of inorganic mercury and electrochemical oxidation of toxic phenolic compounds. Electrochim Acta. 2015;180:1023–32.
52. Abaza A, Mahmoud G, Elsheikh B. Effect of gold nanocomposite on the cytotoxicity of human cancer cell lines. J Pharm Pharmacol. 2018;6:729–41.
53. Lorenzo-Anota HY, Zarate-Triviño DG, Uribe-Echeverría JA, et al. Chitosan-coated gold nanoparticles induce low cytotoxicity and low ROS production in primary leucocytes, independent of their proliferative status. Pharmaceutics. 2021;13(7):942.
54. Martínez-Torres AC, Zarate-Triviño DG, Lorenzo-Anota HY, et al. Chitosan gold nanoparticles induce cell death in HeLa and MCF-7 cells through reactive oxygen species production. Int J Nanomed. 2018;13:3235–50.